Discover Atmosphere

RESEARCH Open Access

Hemispheric warming asymmetry and its contribution to El Niño and Southern Oscillation

Nabil Swedan[1*]

*Correspondence:
Nabil Swedan
nabilswedan@yahoo.com;
swedan@pacificengineeringpllc.com
[1]Pacific Engineering PLLC, 9350 Red-Wood Rd. NE, B210, Redmond, WA 98052, USA

Abstract

Traditional theory treats El Niño event and the subsequent sea temperature oscillation as a self-sustaining process, which is thermodynamically unrealistic, as it overlooks the need for an external energy source. Moreover, current models do not capture key features of the observed Oceanic Niño Index (ONI), making long-term prediction of El Niño events a persistent challenge. This study proposes that hemispheric asymmetry in sea surface warming gives rise to El Niño events. During these events, tropical winds are significantly weakened, allowing wind thrust and momentum flux to generate potential energy cycles in the tropical atmosphere. Fluctuations in this potential energy produce the sea warm and cold phases, characteristic of El Niño Southern Oscillation (ENSO). A theoretical equation for ONI is derived from this framework and demonstrates consistency with observational data. As the hemispheric imbalance in surface warming continues to intensify, the frequency of El Niño events and associated climate extremes is expected to rise over time. This emerging trend may potentially be attributed to anthropogenic influences, which warrant further investigation.

Keywords Atmosphere, El Niño, Ocean, Oceanic Niño Index, Theoretical model

1 Introduction

El Niño is a major climatic phenomenon, capable of disrupting weather patterns across the globe. The energy associated with a single El Niño event is comparable to that released by all tropical typhoons in one year, underscoring its global significance. It can trigger a wide range of severe events, including droughts, floods, extreme temperatures, and shifts in tropical cyclone activity. These impacts are often felt thousands of kilometers around the globe from El Niño location.

Reference [1] provides a detailed account of El Niño events, describing their formation, regional occurrence, economic consequences, and historical significance. El Niño–Southern Oscillation (ENSO) related weather extremes—ranging from heavy rainfall to prolonged drought—have affected communities across the globe. The authors of ref. [2] note a correlation between ENSO phases and the frequency of flood events in Southeast

Asia and beyond. ENSO also influences tropical cyclone activity: Koltzbach [3, 4] analyzed historical records and found that during El Niño phases, typhoon counts tend to rise while hurricane counts decrease. The opposite is observed during La Niña episodes. These inverse relationships emphasize ENSO's broad and complex influence on atmospheric systems and the necessity of understanding its mechanisms.

Scientific understanding of ENSO has advanced considerably over recent decades. Studies in refs. [5, 6] offer detailed syntheses of ENSO dynamics, theoretical progress, and the current state of climate modeling. A widely accepted perspective attributes ENSO to self-sustaining ocean–atmosphere oscillations that regulate thermocline depth anomalies through internal feedback processes. However, as argued in [7], this framework does not fully capture ENSO's pronounced nonlinear behavior. Moreover, the concept of a self-sustaining oscillator raises thermodynamic concerns, as sustained oscillations require an external energy source. Hayashi et al. [8] further note that although contemporary climate models can reproduce observed sea surface temperature anomalies, they struggle to represent the asymmetry between warm and cold phases and lack predictive skill beyond approximately six months.

In this work, a new hypothesis is explored: that the uneven warming between Earth's hemispheres [9] induces heat cycles in the hydrosphere [4], creating warm water anomalies in the tropical Pacific. This is because global warming is not evenly spread across the hydrosphere; tropical basins warm less than the global average. Therefore, sea water thermal expansion is least in these basins. As a result, they have become low areas, where heat from warm water accumulates. When tropical winds are weakened, warm water in tropical basins accumulates west of South America. As the heat becomes sufficiently large, tropical winds (easterlies) weakens further or even arrested during El Niño [10], leading to momentum fluxes and the formation of potential energy cycles in the tropical atmosphere. These cycles induce heat exchange with ocean waters, generating alternating warm and cold sea surface temperature episodes (El Niño and La Niña, respectively) that persist beyond the El Niño peak phase.

Accordingly, heat transfer between the hemispheres is calculated, allowing for the estimation of El Niño-related heat accumulation. A theoretical analysis of the atmosphere–ocean interaction is carried out, leading to the derivation of the final governing equations for Oceanic Niño Index. These equations are then evaluated against available data and observations, showing an agreement (Figs. 1 and 2). The findings support the conclusion that uneven hemispheric warming plays a significant role in driving the El Niño phenomenon and the subsequent El Niño–Southern Oscillation.

This paper presents a comprehensive ENSO related study that includes data and methods, results, theoretical foundations, sample calculations, error analysis, and discussion of the findings. Given the multidisciplinary nature of the research, a dedicated section entitled "Symbols and abbreviations" is included. This section provides definitions and explanations of all symbols used throughout the paper.

2 Data and methods

El Niño Southern Oscillation is monitored using multiple indices that quantify sea surface temperature (SST) anomalies in the tropical Pacific. Among these, the Oceanic Niño Index (ONI) is the most widely used. It measures SST anomalies in Region 3.4, located between 5°N–5°S and 120°W–170°W, where temperature deviations are typically most

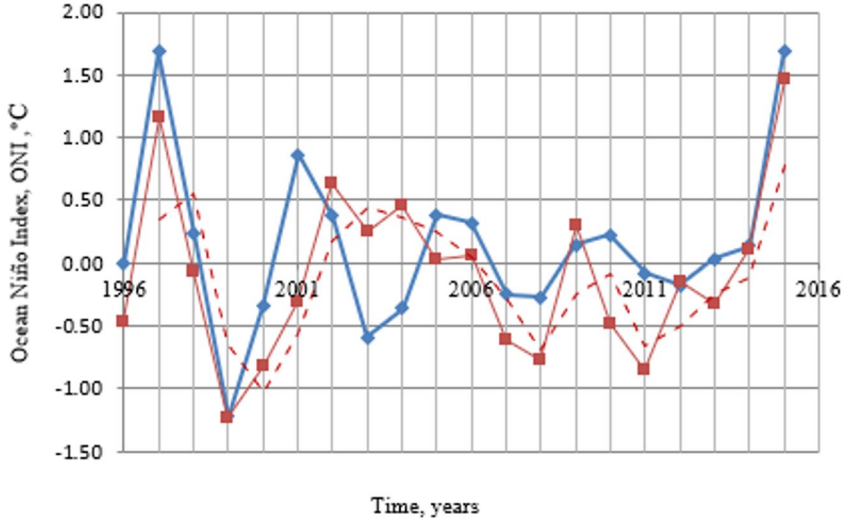

Fig. 1 Observed (solid red lines) and calculated (blue lines) of the annual average value of the Oceanic Niño Index, Niño region 3.4, in degrees C with time. The dashed lines in red color are two-year moving average of the observed index. Data source is National Oceanic and Atmospheric Administration [11]

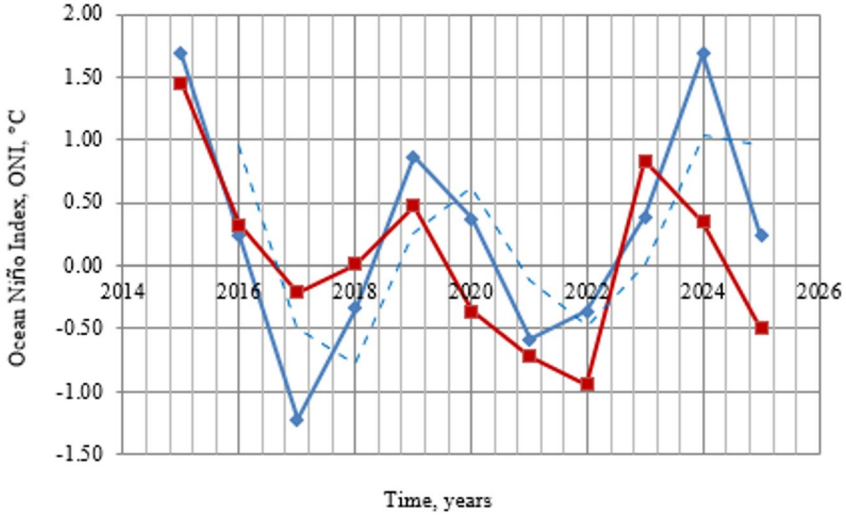

Fig. 2 Projected annual average Oceanic Niño Index (ONI), Niño region 3.4, in degrees C for the period of time between 2015 and 2025 (solid blue lines). The lines in red color are the progressively observed annual average values of the index. The dashed blue lines are two-year moving average of the projected index. Data source is National Oceanic and Atmospheric Administration [11]

pronounced. Following [11, 12], ONI values are interpreted as: Neutral, ± 0.5 °C or less; El Niño (warm phase), greater than + 0.5 °C; La Niña (cool phase), less than - 0.5 °C. El Niño events, which involve significant energy exchange with the atmosphere and ocean, are typically characterized by instantaneous ONI values exceeding 2 to 2.5 °C.

However [11] reports ONI data on a quarterly moving average basis. Sea surface temperature for November, December, and January assumes values about 2 °C or greater during El Niño events. Historical events include the strong episodes of 1996/1997 and 2015/2016 are presented in Fig. 1. The period between two consecutive events (ENSO period) has had a decreasing trend since 1972, averaging 14.6 years.

To support the theoretical model developed in this work, observed key physical parameters relevant to the El Niño region, which varies with every El Niño event, are required. They include:

- Tropopause height (Z): At a typical tropical pressure of 20 kPa and air temperature of 28 °C, the height of the tropical tropopause is estimated as: $Z_T \approx 1.25 \times 10^4$ m [11, 13].
- Evaporation rate (E): Due to limited direct observational data in El Niño region, evaporation is estimated using [14] for a sea surface temperature of 28 °C, yielding: $E \approx 6.08$ mm/day, with a calculation relative error of ± 0.09.
- Humidity and specific heat: At saturation and 28 °C, tropical air holds approximately: 0.0238 kg of water per kg of dry air with a specific heat of: C_P= 1 000 J/kg °C [15]. W_s is thus approximately equal to 0.0238.
- Air density (δ): At 50 kPa, representative mid-troposphere pressure, air density $\delta \approx 0.691$ kg/m³ [13]. For tropical mid-troposphere pressure, air density is approximated as: $\delta_n \approx 0.633$ kg/m³.

The spatial extent of significant El Niño warming is based on reference [16], where the phenomenon affected 70–80% of the tropics, extending from ± 23.4° latitude and 70°W to 180°E for the period 1980–1998. This yields an effective El Niño surface area $A_n \approx 4.91 \times 10^{13}$ m² for that period. The total heat associated with a full ENSO period, Q_{sn}, is referred to as El Niño heat. The value of Q_{sn} is nearly 7.05×10^{21} J, as shown in the sample calculations (Table 1).

The methodology calculates theoretical Oceanic Niño Index (ONI) values in accordance with the derived Eqs. (12) and (20), as well as data provided in this section. As required by the equations, the values of E, M_n, dm/dt have to be determined first. The determination steps are described in the section "Sample calculations." The calculated

Table 1 Calculation of heat anomaly in El Niño region, El Niño heat Q_{sn}, for the period of time between 1997 and 2015

Line No.	Year	Temperature anomaly NH, ˚C	Temperature anomaly SH, ˚C	T_{SH}-T_{NH} ˚C	Cumulative Heat, J
1	1997	–	–	–	0.00E+00
2	1998	0.540	0.479	-0.061	1.60E+20
3	1999	0.306	0.247	-0.059	3.15E+20
4	2000	0.329	0.231	-0.098	5.73E+20
5	2001	0.430	0.354	-0.076	7.72E+20
6	2002	0.460	0.41	-0.050	9.04E+20
7	2003	0.536	0.385	-0.151	1.30E+21
8	2004	0.550	0.331	-0.219	1.88E+21
9	2005	0.557	0.345	-0.212	2.44E+21
10	2006	0.517	0.338	-0.179	2.91E+21
11	2007	0.461	0.266	-0.195	3.42E+21
12	2008	0.435	0.241	-0.194	3.93E+21
13	2009	0.520	0.442	-0.078	4.14E+21
14	2010	0.557	0.422	-0.135	4.49E+21
15	2011	0.417	0.342	-0.075	4.69E+21
16	2012	0.527	0.376	-0.151	5.09E+21
17	2013	0.555	0.389	-0.166	5.52E+21
18	2014	0.713	0.442	-0.271	6.24E+21
19	2015	0.861	0.553	-0.308	7.05E+21

Data source is [9]

NH: northern hemisphere; SH: southern hemisphere

Oceanic Niño Index values are first compared with the observed ones for the period of time between 1996 and 2015 as shown in Fig. 1. Subsequently, Eqs. (12) and (20) were used to project ahead of time ONI values and the occurrence of El Niño event in 2023, Fig. 2.

Lastly, Large Language Models (LLMs) have been occasionally consulted for concepts' originality and merit, as well as AI assisted copy editing for text grammar, readability, and flow. These models include Ask Ai and ChatGPT. The author generated all original texts, and the final edited texts reflect the original work.

3 Results

Using the derived Eq. (20), a theoretical Oceanic Niño Index (ONI) was computed and compared with observed ONI values [11] for the period 1996–2015 (Fig. 1). The observed ONI includes the effects of multiple external influences, including volcanic activities, solar cycles, global temperature trends, and the tropical cyclone count cycle, whereas the theoretical ONI reflects only the modeled dynamics. Despite these additional influences, the theoretical ONI reproduces the main temporal behavior of the observed index within acceptable error margins.

Referring to the error analysis section, at the beginning of the comparison ENSO period, the maximum amplitude error between the theoretical and observed ONI is ± 0.49 °C, with a corresponding phase angle deviation of ± 8.13°. The amplitude error decreases over time, reaching ± 0.13 °C near the midpoint of the record and further reducing to ± 0.039 °C toward the end of the period, although phase error increases by ± 81.30° and ± 146.37° in ten and 18 years, respectively. When the observed ONI is smoothed using a two-year moving average, the agreement with the theoretical ONI improves substantially, thus supporting the utility of the model. Some deviations are expected, as the theoretical ONI assumes a constant initial condition and does not account for temporal variability in heat sources.

The model's predictive skill decreases with the number of years in consideration. For the early years of ENSO, ONI occurrence may be predicted practical accurately. The prediction error for ten years approaches ± 1 year, and an 18-year prediction would expect an error of ± 2 years. Figure 2 shows that El Niño event of 2023 could have been predicted 8 ± 1 years ahead of time.

The solution of Eq. (20) yields a damped and asymmetric oscillation, characterized by stronger warm phases relative to cold phases—consistent with observations, but not captured by most existing ENSO models. This asymmetry is in line with observed ENSO behavior and is reproduced without imposing it as a model constraint. The model implies that ENSO is not a self-sustaining oscillation; instead, energy input during El Niño events—primarily from wind thrust and momentum fluxes, created by ocean's heat anomaly—sustains the cycle. This is supported by observations from ref. [17], who noted a decrease in the tropical tropopause height during El Niño phases, indicating fluctuation in atmospheric potential energy.

This work shows a correlation between the frequency of El Niño events and the temperature difference between the northern and southern hemispheres. As this difference increases, so does the frequency of El Niño occurrences. According to the dataset provided by ref. [9], the sea surface temperature difference can be approximated by the following relationship: T_{SH}-T_{NH}=-0.01 x t-0.048, where T_{SH} is the average temperature

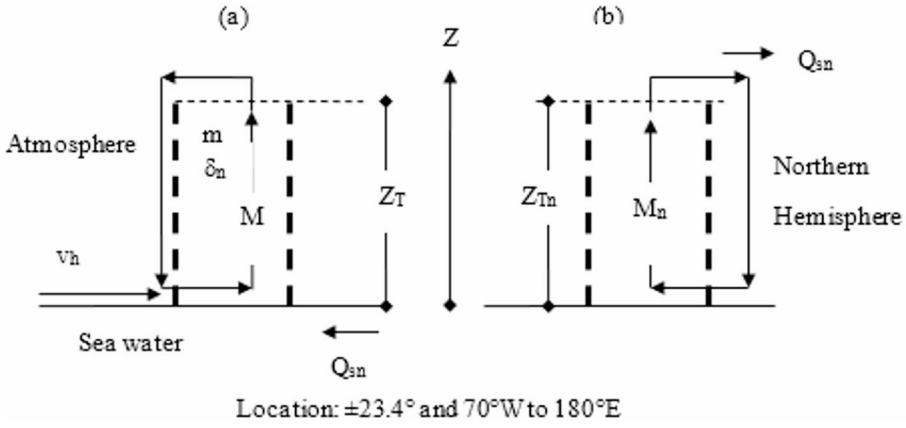

Fig. 3 Heat and mass transfer parameters in El Niño region's atmosphere (volume enclosed by the dashed lines). **a** Steady conditions before and after El Niño event. **b** Steady conditions during El Niño event. M=Vertical component of tropical air mass flow before and after El Niño event, kg s^{-1}; v=Vertical velocity component of tropical winds or air mass in Z direction, m s^{-1}; v_h: Horizontal velocity component of tropical winds, m s^{-1}; Z_T: Height of tropical tropopause or air mass, m; Z_{Tn}: Height of tropical tropopause or air mass during El Niño event, m; Q_{sn}: Solar heat anomaly in El Niño region (El Niño heat), J; M_n: Annual air mass flow during El Niño event, expressed in kg s^{-1}; v_n: Vertical tropical wind velocity or air mass in Z direction during El Niño event, m s^{-1}

of the southern hemisphere, T_{NH} is the average temperature of the northern hemisphere, and t is the number of years since 1997. This trend suggests a rising frequency of El Niño events, consistent with observations in Fig. 1 and projections in Fig. 2. While geographical factors may contribute to the initial temperature asymmetry between the hemispheres, the ongoing increasing trend likely stems from additional causes. Beyond greenhouse gas emissions, human influences such as uneven global population distribution and disparity in energy consumption between the hemispheres are likely contributing factors.

4 Theory and analysis

The atmospheric textbooks [18, 13] provide detailed discussions on atmospheric properties, including thermodynamics, physical forces, and the equations of motion. Based on these principles, the air volume over the El Niño region—defined by the dashed lines in Fig. 3—can experience several forces: buoyant uplift, the Coriolis force, and variation in air mass momentum flux across its boundaries. The latter results in a reactive force, or thrust, acting on the air volume.

Prior to an El Niño event (Fig. 3a), the upward air mass flow rate, denoted as M, is assumed to be in a steady state with a corresponding vertical velocity **v**. During an El Niño event (Fig. 3b), the horizontal components of the tropical surface winds (v_h) decrease significantly and therefore considered negligible as discussed in the introduction section. Under steady-state conditions during the event, the air mass flow rate and vertical velocity are represented as M_n and v_n, respectively.

Prior to the onset of El Niño, the net atmospheric force in Z direction (vertical to the surface) may be written as follows:

$$F_z = F_b + F_{cz} + (dm_e/dt)\ v_e - (dm_o/dt)\ v_o \tag{1}$$

where, F_z: Net atmospheric force component in Z direction, N. F_b: Buoyant upward force, N. F_{cz}: Coriolis force component in Z direction, N. m_e: Mass of air entering the air

volume enclosed by the dashed lines, kg. v_e : Velocity of the air mass entering the air volume, m s^{-1}. m_o: Mass of air exiting the air volume, kg. v_o : Velocity of the air mass exiting the air volume, m s^{-1}. t: Time, s.

In Eq. (1), friction forces in Z direction are neglected because air streams move upward, away from the surface. The difference $(dm_e/dt)\ v_e$-$(dm_o/dt)\ v_o$ is equal to the force or thrust imparted by air flow streams in and out of the air volume enclosed by the dashed lines of Fig. 3. This difference is equal to d(m v)/dt, where m is air mass, kg, and v is air mass velocity, m s^{-1}. Equation (1) simplifies

$$F_z = F_b + F_{cz} + d\,(m\ v)\,/dt \tag{2}$$

where, d(m v)/dt: Variation in the flux of air mass momentum with time, N. m: Mass of air in the volume enclosed by the dashed lines of Fig. 3 in El Niño region, kg. v: Velocity or displacement of the air mass, m s^{-1}.

Although the tropical warm air mass in El Niño region is large and straddles the equator, it is only 4% or less of the total mass of the surrounding cooler atmospheric air. Therefore, the force of buoyancy may be expressed as follows:

$$F_b = (\delta - \delta_n)\ A_n Z_T g \tag{3}$$

Where δ: Average density of surrounding air, kg m^{-3}. δ_n: Average air density in El Niño region, kg m^{-3}. A_n: Area of El Niño region, m^2. Z_T: Height of tropical tropopause, m. g: Gravity acceleration, m s^{-2}. The component of the Coriolis force in Z direction, F_{cz}, may be obtained from the total force of Coriolis

$$\mathbf{F_c} = -2\ m\,\boldsymbol{\omega} \times \mathbf{v_r} - 2\ m\,\boldsymbol{\omega} \times \mathbf{dZ}\,(\mathbf{t})\,/\mathbf{dt} \tag{4}$$

Where, $\mathbf{F_c}$: Total force of Coriolis, N. $\boldsymbol{\omega}$: Angular velocity of the earth around its axis, radians s^{-1}. $\mathbf{v_r} = v_h$: Relative horizontal velocity between air mass in El Niño region and surface, m s^{-1}. $\mathbf{dZ(t)/dt}$: Relative vertical velocity between air mass in El Niño region and the surface, m s^{-1}.

The symbols in bold font in Eq. (4) indicate vectors and their cross products. During El Niño, there is no tangible horizontal movement of the air mass m as discussed in introduction. Therefore, air mass relative velocity with respect to the surface, $\mathbf{v_r}$, may be neglected. The first term on the right side of Eq. (4), -2 m $\boldsymbol{\omega} \times \mathbf{v_r}$, may thus be discarded. The second term of the equation, -2 m $\boldsymbol{\omega} \times \mathbf{dZ(t)/dt}$, is always perpendicular to Z and can have no component in Z direction. The term F_{cz} of Eq. (2) may be omitted as well.

At steady state before El Niño event, the net atmospheric force and its components are nearly equal to zero. Therefore, v is about constant ($dv/dt \approx 0$), and the term d(m v)/dt of Eq. (2) simplifies

$$d\,(m\ v)\,/dt\ =\ v\ dm/dt\ +\ m\ dv/dt\ =\ v\ dm/dt \tag{5}$$

At steady state before El Niño event $F_z \approx 0$, and Eqs. 2, 3, and 5 give

$$0 = (\delta - \delta_n)\ A_n Z_T g\ +\ v\ dm/dt \tag{6}$$

Similarly, at steady state during El Niño event, $F_z \approx 0$ and Eqs. 2, 3, and 5 give

$$0 = (\delta - \delta_n)\ A_n Z_{Tn} g\ +\ v_n dm/dt \tag{7}$$

where Z_{Tn}: Height of tropical tropopause during El Niño event, m. v_n: Vertical air velocity or air mass displacement during El Niño event, m s^{-1}.

The right sides of Eqs. (6) and (7) are similar to the right side of Eq. (2). The difference between them is thus equal to variation in atmospheric force, F_z, when air flow decelerates from M at steady state to M_n during El Niño event (Fig. 3a and b). Where M and M_n indicate vertical components of the respective air mass flow. Therefore

$$-dF_z = (\delta - \delta_n)\ A_n Z_{Tn} g\ +\ v_n dm/dt - (\delta - \delta_n)\ A_n Z_T g - v\ dm/dt \tag{8}$$

The differential term $-dF_z$ on the left side of Eq. (8) is equal to $-d(m\ d^2Z/dt^2) = -(dm/dt)\ d^2Z/dt^2 \times dt - m\ d^3Z/dt^3 \times dt$. If air deceleration, $-d^2Z/dt^2$, is assumed to be about constant with time, then $-d^3Z/dt^3 \approx 0$ and $-dF_z \approx -(dm/dt)\ d^2Z/dt^2\ dt$. The term (dm/dt) of this equation represents the increase in air mass above El Niño region that is required to remove El Niño heat from sea water. It is equal to the air mass flow rate M_n as required by the air mass balance of the volume enclosed by the dashed lines of Fig. 3b. Therefore, $-dF_z \approx -M_n d^2Z/dt^2\ dt$. If the period of time, dt, is selected to be equal to the time required for one complete El Niño event, or one year as will be discussed later in this section, Eq. (8) yields the following relationship:

$$-M_n d^2Z\,(t)\,/dt^2 = (\delta - \delta_n)\ A_n\,(Z_{Tn} - Z_T)\ \ g\ +\ dm/dt\ \ (v_n - v) \tag{9}$$

where M_n: Annual air mass flow rate during El Niño, kg yr^{-1}.

The difference, $(Z_{Tn}\text{-}Z_T)$, represents variation in the height, ξ(t), of the tropopause or air mass above sea water in El Niño region. The difference $(v_n\text{-}v)$ is equal to dξ(t)/dt. Consequently, Eq. (9) gives

$$M_n d^2\xi\,(t)\,/dt^2 + (dm/dt)\ \ d\xi\,(t)\,/dt + (d - d_n)\ A_n g \xi\,(t)\ =\ 0 \tag{10}$$

where ξ(t): Variation in the height of tropical tropopause or air mass in El Niño region, m.

Equation (10) is a differential equation of the second order, and its solution requires two initial conditions. Specifically, initial ENSO phase angle and amplitude. These conditions may be obtained from the observed Oceanic Niño Index (Fig. 1). The initial phase angle may be assumed to be equal to zero at time t = 0. Nearly one year (1997 to 1998) was required to remove El Niño solar heat anomaly. This may be explained in analogy to removing seasonal variation and tropical cyclone heat anomalies. They too require one year to completion. Based on this discussion and Fig. 1, at time t = 1 year, ENSO phase angle is 90°, ENSO amplitude ξ(t) = ξ_0, and

$$\xi\,(t) = \xi_0 Exp\,[-\,(dm/dt)\ \ t/2M_n]\ \ \times\ \sin\,[t\{(\delta - \delta_n)\ A_n g/M_n - \{(dm/dt)\,/2M_n\}^2\}^{0.5}] \tag{11}$$

$$\xi\,(t)\,/\xi_0\ =\ Exp\,[-\,(dm/dt)\ \ t/2M_n]\ \ \times\ \sin\,[t\{(\delta - \delta_n)\ A_n g/M_n - \{(dm/dt)\,/2M_n\}^2\}^{0.5}] \tag{12}$$

where ξ_0: Initial amplitude of the air mass oscillation in El Niño region, m. ξ(t): Instantaneous amplitude of the air mass oscillation, m.

On the other hand, variation in air mass height dZ(t) and variation in surface heat are correlated. When an air parcel having unit mass gains heat, dQ_A, from the surface, the air internal energy and potential energy increase in accordance with the first law of thermodynamics [19]:

$$dQ_A = dU + dW \tag{13}$$

$$-dQ_S = dQ_A \tag{14}$$

dQ_A: Heat gained by unit air mass, J kg^{-1}. dU: Internal energy gained by unit air mass, J kg^{-1}. dW: Work (potential energy) produced by unit air mass, J kg^{-1}. $-dQ_S$: Heat lost by the surface per unit air mass, J kg^{-1}.

$$-dQ_S = dQ_A = dU + g\, dZ\,(t)/2 \tag{15}$$

The division of dZ(t) by 2 in Eq. (15) is required because the potential energy must be calculated at average variation in air mass height. Because heat exchange with the atmosphere is a frictionless thermodynamic process that occurs infinitesimally with time, equilibrium and equipartition of energy is the result, and dU = g dZ(t)/2. Therefore, Eq. (15) gives $-dQ_S$=2 g dZ(t)/2 = g dZ(t). Or, variation in potential energy of atmospheric air mass is equal to the opposite sign of variation in surface heat. This correlation may be used to convert fluctuation in the height of the air mass [ξ(t) = dZ(t)] of Eq. (11) into variation in surface heat as follows:

$$Q_s\,(t) = Q_{sn} \times \xi\,(t)/\xi_0 \tag{16}$$

Where Q_s(t): Instantaneous variation in heat content of sea water in El Niño region, J. Q_{sn}: El Niño heat, or initial sea water heat anomaly, J yr^{-1}.

The fluctuations of the instantaneous heat, Q_s(t), produces ENSO warming and cooling episodes in El Niño region, damped with time, long after the entire El Niño heat Q_{sn} has been removed from sea water. To calculate sea temperature variation of these episodes, the following heat and mass balance may be used:

$$\Delta T_{sn} = Q_s\,(t)/[M\ C_p] \tag{17}$$

$$E = M(W_s - W_t) \tag{18}$$

where, ΔT_{sn}: Variation in average sea surface temperature in El Niño region, which is equal to the variation in sea surface air temperature in the region, °C. M: Annual average surface air flow rate in El Niño region, kg yr^{-1}. C_p: Air specific heat, J kg^{-1} $°C^{-1}$. E: Annual average evaporation in El Niño region, kg yr^{-1}. W_s: Air humidity at saturation with tropical sea water, kg water per kg dry air, dimensionless. W_t: Air humidity at the tropopause, 0.0 kg water per kg dry air, dimensionless.

The value of ΔT_{sn} is an average sea temperature anomaly for the entire El Niño region. At the equator where Niño region 3.4 is defined (see data section), sea surface temperature observes maximum anomaly, which may be assumed to be equal to $2\Delta T_{sn}$. The temperature anomaly in Niño region 3.4, $2\Delta T_{sn}$, is by definition equal to the Oceanic Niño Index. By eliminating M from equations (17), the instantaneous index value may be presented as follows:

$$\text{Instantaneous Oceanic Niño Index (ONI)} = 2\Delta T_{sn} = 2 \times Q_{sn} \times [\xi\,(t)/\xi_0] \times W_s/(E\ C_p) \tag{19}$$

Multiplying the right side of Eq. (19) by 2/π, the average value of the index follows:

$$\text{Average ONI} = (4/\pi) \times Q_{sn} \times [\xi\,(t)/\xi_0] \times W_s/(E\ C_p) \tag{20}$$

5 Sample calculations

Parameterization of energy cycles methodology as explained by ref. [4] may be utilized to calculate heat imbalance between the hemispheres. From Eqs. (1), (2), (3), and sample calculations of this reference [4], the heat calculation is quoted as follows:

$$\Delta h_f = \beta d_m (T_{SH} - T_{NH}) \tag{21}$$

$$\Delta Q_n = -[\{(0.2 + \Delta h_f)/0.2\}^{0.5} - 1] \times Q_{PHT} \tag{22}$$

where h_f: Available average liquid elevation for the thermohaline brine flow, 0.2 m. β: Sea water volumetric thermal expansion, 200×10^{-6} °C^{-1}. d_m: Average depth of ocean mixed layers, 95 m. T_{SH}: Average annual sea temperature of the southern hemisphere, °C. T_{NH}: Average annual sea temperature of the northern hemisphere, °C. ΔQ_n: Calculated annual heat exchanged between the hemispheres, J yr^{-1}. Q_{PHT}: Poleward heat transport, 5.52×10^{22} J yr^{-1}."

The cumulative value of the annual heat between two consecutive El Niño events is equal to El Niño heat Q_{sn}. In Table 1 the value of Q_{sn} is calculated for the period of time between the events that occurred in 1997 and 2015. The difference in sea temperature between the hemispheres is provided by ref. [9]. They are given as sea temperature anomalies for the northern and southern hemispheres. The difference between them is equal to (T_{SH}-T_{NH}) required for Eq. (21). For the year 1998, (T_{SH}-T_{NH}) = -0.061 and ΔQ_{1998} = -[{(0.2 + 200 × 10^{-6} × 95 × 0.061)/0.2}$^{0.5}$-1] × 5.52 × 10^{22} = 1.60 × 10^{20} J. The calculation is repeated every year through 2015, and the cumulative value of ΔQ_n is approximately equal to 7.05×10^{21} J. This is the amount of solar heat anomaly of El Niño, indicated as El Niño heat Q_{sn} in the data section. The heat accumulates in El Niño region, characterized for being low location as explained in Introduction.

Required for the application of Eq. (20) is the value of dm/dt, which is part of the decay factor of the oscillation (dm/dt)/2M_n. The value of dm/dt is a constant, dictated by astronomical parameters and represents variation in the mass of atmospheric air for any given latitude in one year. For El Niño region, the value of dm/dt is equal to the variation in air mass of the volume enclosed by the dashed lines of Fig. 3 in one year, during which air having density δ_n is replaced by surrounding air having density δ

$$dm/dt \approx \Delta m/\Delta t = (\delta V - \delta_n V)/t \tag{23}$$

$$dm/dt \approx [(\delta - \delta_n)\ A_n Z_T]/\tau \tag{24}$$

where V: Volume of the air mass above sea water in El Niño region, m^3. τ: Time, one year, yr.

Example Evaporation caused by El Niño heat, E_n = Q_{sn}/Latent heat of water evaporation, E_n = Q_{sn}/(2.44 × 10^6) = 7.05 × 10^{21}/(2.44 × 10^6) = 2.89 × 10^{15} kg yr^{-1}.

Because gravity acceleration used in m s^{-2}, all flow rates must be rated per second as well. One year is equal to 3.15×10^7 seconds.

Air flow rate during El Niño, M_n = E_n/W_s = 2.89 × 10^{15}/(0.0238 × 3.15 × 10^7) = 3.85 × 10^9 kg s^{-1}, Eq. (18). dm/dt = (δ–δ_n) A_n Z_T/(3.15 × 10^7) = (0.691–633) × 4.91 × 10^{13} × 1.25 × 10^4/(3.15 × 10^7) =1.14 × 10^9 kg s^{-1} , Eq. (24).

Argument terms of the sinusoidal function, Eq. (12):

$$(\delta - \delta_n)\ A_n g/M_n = (0.691 - 0.633)\ \times\ 4.91\ \times\ 10^{13} \times\ 9.8/\ 3.85\ \times\ 10^9 = 7\ 248.95$$

$$\{(dm/dt)/2M_n\}^2 = \left\{\left(1.14\ \times\ 10^9\right)/\left(2\ \times\ 3.85\ \times\ 10^9\right)\right\}^2 = 0.02$$

For 1997, t = 1 year

Oscillation decay factor, $(dm/dt) \times t/2M_n = (1.14 \times 10^9) \times 1/(2 \times 3.85 \times 10^9) = 0.148$.

Angle of the sinusoidal function, $[t \times \{(\delta - \delta_n)\ A_n\ g/M_n - \{(dm/dt)/2M_n\}^2\}^{0.5}] = [1 \times \{7248.95. - 0.02\}^{0.5}] = 85.14°$, Eq. (12).

$\xi(1)/\xi_0 = \text{Exp}\ [-0.148]\ \sin\ [85.14] = 0.86$, Eq. (12).

$Q_s(1) = Q_{sn} \times \xi(1)/\xi_0 = 7.05 \times 10^{21} \times 0.86 = 6.06 \times 10^{21}$ J yr^{-1}, Eq. (16).

Average annual evaporation in tropics, E = 6.08 mm d^{-1}, data section.

Average annual evaporation in El Niño region, E = 6.08 mm $d^{-1} \times 365$ (d yr^{-1}) $\times A_n = 6.08 \times 365 \times 4.91 \times 10^{13} = 1.09 \times 10^{17}$ kg yr^{-1}.

Air mass flow rate in El Niño region, $M = E/W_s = 1.09 \times 10^{17}/0.0238 = 4.58 \times 10^{18}$ kg yr^{-1} (1.45×10^{11} kg s^{-1}), Eq. (18).

Oceanic Niño Index (ONI) for 1997 = $2 \times Q_s(1) \times W_s/[E \times C_p] = 2 \times 6.06 \times 10^{21} \times 0.0238/(1.09 \times 10^{17} \times 1000) = 2.65$ °C, Eq. (19).

Average Oceanic Niño Index (ONI) for 1997 = $4/\pi \times Q_s(1) \times W_s/[E \times C_p] = 4/\pi \times 6.06 \times 10^{21} \times 0.0238/(1.09 \times 10^{17} \times 1000) = 1.68$°C, Eq. (20).

Similar calculations are conducted for the years between 1998 and 2015, and the plot of the calculated average ONI is presented in Fig. 1 in blue color. The same procedure is repeated to predict the occurrence of El Niño event of 2023, blue lines of Fig. 2.

6 Evaluation of calculation error

A measured or calculated quantity x is assumed to have error absolute value Δx and relative error εx = Δx/x. The maximum absolute error value is indicated as Max Δx. The relative error of evaporation, εE, is nearly ± 0.09, data section. Because $M_n = E_n/W_s$, Eq. (18), then the relative error $\varepsilon M_n = \pm 0.09$. The value of the theoretically calculated poleward heat transport, Q_{PHT}, has an accuracy of ± 0.20 [4]. Because El Niño heat, Q_{sn}, is a fraction of the poleward heat transport, its relative error εQ_{sn} is ± 0.20 as well.

For the argument of sinusoidal function, the symbol θ will be used, and $\theta = t[(\delta - \delta_n)\ A_n\ g/M_n - \{(dm/dt)/2M_n\}^2]^{0.5}$, Eq. (11). Neglecting the second term of the argument based on the sample calculation, then $\theta \approx t[(\delta - \delta_n)\ A_n\ g/M_n]^{0.5}$ and error of θ follows:

$$\Delta\theta = 0.5\ t\left[(\delta - \delta_n)\ A_n g/M_n\right]^{-0.5} \times\ \left[(\delta - \delta_n)\ \Delta A_n g/M_n - (\delta - \delta_n)\ A_n g\ \left(-\Delta M_n/M_n^2\right)\right]$$

$$\Delta\theta = 0.5\ t\left[(\delta - \delta_n)\ A_n g/M_n\right]^{-0.5} \times\ \left[(\delta - \delta_n)\ A_n \varepsilon A_n g/M_n + (\delta - \delta_n)\ A_n g\ \varepsilon M_n/M_n\right]$$

$$\Delta\theta = 0.5\ \times\ t\left[(0.691 - 0.633)\ \times\ 4.91\ \times\ 10^{13} \times\ 9.8/3.85\ \times\ 10^9\right]^{-0.5} \times\ \left[(0.691 - 0.633)\ 4.91\ \times\ 10^{13} \varepsilon A_n 9.8/3.85\ \times\ 10^9 + (0.691 - 0.633)\ 4.91\ \times\ 10^{13} \times\ 9.8\ \times\ (\pm 0.09)/3.85\ \times\ 10^9\right]$$

$$\Delta\theta = 0.5\ \times\ t\ [0.0118]\ \times\ [7\ 248.95 \varepsilon A_n \pm 652.41]$$

For $\varepsilon A_n = \pm 0.1$, $\Delta\theta = \pm 8.13$ t

For t=1 or 1997, $\Delta\theta = \pm 8.13^\circ$

For t = 10 or 2006, $\Delta\theta = \pm 81.30^\circ$

For t=18 or 2014, $\Delta\theta = \pm 146.37^\circ$

The calculated error of the Oceanic Niño Index (ONI) may be analyzed:

$\xi\,(\mathrm{t})\,/\xi_0 = \mathrm{Exp}\,[-\,(\mathrm{dm/dt})\ \mathrm{t}/2\mathrm{M_n}]\ \times\ \sin\,[\theta]$, Eq. (12).

$\xi\,(\mathrm{t})\,/\xi_0 = \mathrm{Exp}\left[-1.14\ \times\ 10^9 \times \mathrm{t}/\left(2\ \times\ 3.85\ \times\ 10^9\right)\right] = \mathrm{Exp}\,[-0.148\ \mathrm{t}]$

$\mathrm{ONI} = (4/\pi)\ \times\ \mathrm{Q_{sn}} \times\ [\xi\,(\mathrm{t})\,/\xi_0]\ \times \mathrm{W_s}/(\mathrm{E}\ \mathrm{C_p})$, Eq. (20).

The absolute value of the error $\Delta[\xi(t)/\xi_0]$ is negligible.

For $\theta = n \times \pi/2$, the absolute value of the maximum error of ONI follows:

$$\begin{aligned}\mathrm{Max}\ \Delta\,(\mathrm{ONI}) = {} & (4/\pi)\ \times\ \Delta\mathrm{Q_{sn}} \times [\xi\,(\mathrm{t})\,/\xi_0]\mathrm{W_s}/(\mathrm{E}\ \mathrm{C_p}) \\ & + (4/\pi)\ \times\ \mathrm{Q_{sn}} \times\ [\xi\,(\mathrm{t})\,/\xi_0]\ \times \mathrm{W_s}/\mathrm{C_p} \times (-\Delta\mathrm{E}/\mathrm{E}^2)\end{aligned}$$

$$\begin{aligned}\mathrm{Max}\ \Delta\,(\mathrm{ONI}) = {} & (4/\pi)\ \times\ \Delta\mathrm{Q_{sn}} \times (\mathrm{Q_{sn}}/\mathrm{Q_{sn}})\ [\xi\,(\mathrm{t})\,/\xi_0]\mathrm{W_s}/(\mathrm{E}\ \mathrm{C_p}) \\ & + (4/\pi)\ \times \mathrm{Q_{sn}} \times [\xi\,(\mathrm{t})\,/\xi_0]\ \times \mathrm{W_s}/(\mathrm{E}\ \mathrm{C_p})\ \times (-\varepsilon\mathrm{E})\end{aligned}$$

$$\mathrm{Max}\ \Delta\,(\mathrm{ONI}) = (4/\pi)\ \times\ \mathrm{Q_{sn}}\mathrm{Exp}\,[-0.148\ \mathrm{t}]\ \times \mathrm{W_s}/(\mathrm{E}\ \mathrm{C_p})(\varepsilon\mathrm{Q_{sn}} -\ \varepsilon\mathrm{E})$$

$$\begin{aligned}\mathrm{Max}\Delta\,(\mathrm{ONI}) = {} & (4/\pi)\ 7.05\ \times\ 10^{21} \times\ \mathrm{Exp}\,[-0.148\ \mathrm{t}] \\ & \times\ 0.0238/\left(1.09\ \times\ 10^{17} \times\ 1\ 000\right)\ \times\ (0.2 - 0.09)\end{aligned}$$

$$\mathrm{Max}\Delta\,(\mathrm{ONI}) = \pm 0.57\ \times\ \mathrm{Exp}\,[-0.148\ \mathrm{t}]$$

For t=1, or 1997, $\mathrm{Max}\ \Delta\,(\mathrm{ONI}) = \pm 0.49\ ^\circ\mathrm{C}$

For t=10, or 2006, $\mathrm{Max}\ \Delta\ (\mathrm{ONI}) = \pm 0.13\ ^\circ\mathrm{C}$

For t=18, or 2014, $\mathrm{Max}\ \Delta\ (\mathrm{ONI}) = \pm 0.039\ ^\circ\mathrm{C}$

7 Discussion

This work presents a physically motivated model of ENSO dynamics based on heat imbalance between the hemispheres, resulting in hydrospheric heat cycles that culminate in El Niño events. These events act as periodic energy injections, maintaining the ENSO cycle.

Based on the results section, Eq. (20) provides a reasonable match (within error margins) with observed ONI values from 1996 to 2015, particularly when smoothed over a two-year moving average. It successfully replicates key features such as phase asymmetry and nonlinearity, which are often missed by conventional models.

Using this theoretical model, ONI values were projected for 2015–2024 (Fig. 2), with an estimated accuracy of ± 1 year. Figure 2, confirms that ENSO period has decreased, from an average of 14.6 years (data section) to eight years, as expected from the model. Eight years has been the shortest ENSO period on record, a potential concern moving forward.

The data used to generate Fig. 2 were those for the period 1980–1998. For improved accuracy, actual data for 2015 should be used, in particular El Niño area and heat anomaly. In addition, the influence of external drivers like volcanic eruptions, solar cycles,

surface temperature rise, and tropical cyclone variability should be considered for intra-annual values of ONI.

Contrary to prevailing assumptions, ENSO is not a self-sustaining phenomenon. Energy is supplied during El Niño events through wind-induced potential energy cycles in the tropical atmosphere.

Finally, there is room for improvement: The model currently uses an annual scale to minimize seasonal noise. However, it may be extended to monthly or quarterly timescales with proper adjustment for seasonal heat transport and Earth's orbital dynamics. More accurate estimates of parameters such as surface evaporation, El Niño heat, and El Niño region area for each oscillation may improve further model accuracy.

List of symbols

A_n	Surface area affected by El Niño warming event, m^2
β	Volumetric thermal expansion of sea water, $°C^{-1}$
C_p	Specific heat of air mixture, J kg^{-1} $°C^{-1}$
d	A symbols that denotes an infinitesimal variation
ε	Relative error of measurement or calculated parameter
Δ	Small variation or absolute error in measurement or calculation
d^{-1}	Per day
δ	Average density of the atmosphere air, kg m^{-3}
δ_n	Average density of the atmospheric air in El Niño region, kg m^{-3}
E	Evaporation in El Niño region before and after El Niño event, kg yr^{-1}
ENSO period	Time in years between two consecutive El Niño events
E_n	Evaporation in El Niño region during El Niño event, kg s^{-1}
Exp (x)	Exponential function of natural logarithm base, equal to e^x
F_z	Component of the resultant of atmospheric force in Z direction, N
F_b	Force of air buoyancy, N
Fc	Force of Coriolis, N
g	Gravity acceleration, m s^{-2}
m	Mass of air between sea level and tropical tropopause in El Niño region, Kg
M_n	Air mass flow rate in El Niño region during El Niño event, kg s^{-1}
M	Air mass flow rate in El Niño region before and after El Niño event, kg s^{-1}
n	Number of years between two consecutive El Niño events, years
N	Newton
ONI	Oceanic Niño Index, °C
P	Pressure of the atmosphere, kPa
Q_A	Heat gained by an arbitrary air mass, J kg^{-1}
Q_S	Heat removed from the surface by an arbitrary air mass, J kg^{-1}
ΔQ_n	Annual heat accumulation in El Niño region, J
Q_{PHT}	Poleward heat transport, 5.52×10^{22} J yr^{-1}
Q_{sn}	Cumulative annual heat in El Niño region in n years, J
$Q_S(t)$	Heat anomaly of sea water in El Niño region, J
s	Second
t	Time in years
τ	Earth's revolution time around the sun, 3.15×10^7 s
T_{NH}	Average sea temperature of the northern hemisphere, °C
T_{SH}	Average sea temperature of the southern hemisphere, °C
T_{sn}	Sea temperature in El Niño region, °C
U	Internal energy of an arbitrary air parcel, J
V	Volume of air mass, m^3
v	Vertical component of air velocity or air mass in El Niño region, m s^{-1}
v_h	Horizontal component of air velocity in El Niño region, m s^{-1}
v_n	Vertical component of air velocity or air mass in El Niño region during El Niño event, m s^{-1}
V_r	Relative velocity between air mass in El Niño region and surface, m s^{-1}
W	Work produced by an arbitrary air mass, J kg^{-1}
W_s	Surface air humidity at saturation, kg water per kg dry air
W_t	Air humidity at tropical tropopause, 0 kg water per kg dry air
ω	Angular velocity of the earth around its rotational axis, radians s^{-1}
yr	Year
Z	Vertical coordinate, height above sea level, m
Z_T	Height of tropical tropopause or air mass, m
ξ	Fluctuation in the height of tropopause Z_T or air mass above sea water, m

Acknowledgements
I sincerely thank the Editor, Assistant Editor, article production team, and anonymous reviewers for their time and valuable comments, without which this publication would not have been possible.

Author contributions
The author, Nabil Swedan, produced the entire work including original text and figures.

Funding
This work was funded by the author.

Data availability
The data on hemispheric temperature rise is available at https://www.metoffice.gov.uk/hadobs/hadsst4/data/download.html. The Oceanic Niño Index data is available at https://www.cpc.ncep.noaa.gov/products/analysis_monitoring/ensostuff/ONI_v5.php.

Declarations

Ethics approval and consent to participate
Ethical approval was not required for this study, as it did not involve human participants or animals. No human participants or animals were involved in this study; therefore, consent to participate was not required.

Consent for publication
Not applicable.

Competing interests
The authors declare no competing interests.

Received: 15 October 2025 / Accepted: 14 February 2026
Published online: 02 March 2026

References

1. Caviedes CN. El Niño in history storming through the ages. Gainesville. Florida, U.S.A.: University Press of Florida; 2001. p. 279.
2. Ward PJ, Kummu M, Lall U. Flood frequencies and durations and their response to El Niño Southern Oscillation: Global analysis. J Hydrol. 2016;529:358–78. https://doi.org/10.1016/j.jhydrol.2016.05.045.
3. Koltzbach PJ. El Niño-Southern Oscillation's Impact on Atlantic Basin Hurricanes and U.S. Landfalls. J Clim. 2011;24:1252–63. https://doi.org/10.1175/2010JCL13799.1.
4. Swedan N. Parameterization of energy cycles between the hemispheres. Sci Prog. 2020. https://doi.org/10.1177/0036850420922773.
5. Wang C, Deser C, Yu JY, et al. El Niño-Southern Oscillation (ENSO): A review. In: Glymn P, Manzello D, Enochs I, editors. Coral Reefs of the Eastern Pacific. Dordrecht: Springer Science; 2016. pp. 85–106. https://doi.org/10.1007/978-94-017-7499-4_4.
6. Wang C. A review of ENSO theories. Natl Sci Rev. 2018;5:813–25. https://doi.org/10.1093/nsr/nwy104.
7. An IS, Jin FF. Nonlinearity and Asymmetry of ENSO. J Clim. 2004;17(2):2399–412.
8. Hayashi M, Jin FF, Stuecker MF. Dynamics for El Niño-La Niña asymmetry constrains equatorial-Pacific warming pattern. Nat Commun. 2020;11:4230. https://doi.org/10.1038/s41467-020-17983-y.
9. Temperature CRU. Temperature data (HadCRUT4, CRUTEM4) climate research, under tab Data for downloading and file formats, HadSST4, Version 4.0.1.0, Norwich, U. K.: University of East Anglia, Climate Research Unit; 2025. https://www.metoffice.gov.uk/hadobs/hadsst4/data/download.html. Accessed 5 Apr 2025.
10. Rasmusson EM, Carpenter TH. Variations in tropical sea surface temperature and surface wind fields associated with the Southern Oscillation/El Niño. Mon Weather Rev. 1982;110:354–84..
11. NOAA. Description of Changes to Ocean Niño Index, Climate Prediction Center-ONI-NOAA, Cold & Warm Episodes by Season, Centered 30-year base period. Manchester: National Oceanic and Atmospheric Administration; 2025. https://www.cpc.ncep.noaa.gov/products/analysis_monitoring/ensostuff/ONI_v5.php. Accessed 10 Apr 2025.
12. NCAR. Climate Data (Nino 1+2, 3, 3.4, 4; ONI and TNI). Boulder: National Center for Atmospheric Research; 2023. https://climatedataguide.ucar.edu. Accessed 15 Oct 2023.
13. Fleagle RG, Businger JA. In: Van Mieghem J, Hales AL, editors. An Introduction to atmospheric physics. Vol. 52, 2 ed. New York: Academic; 1980. p. 432.
14. Swedan NH. Calculation of Open Water Evaporation as a Climate Parameter. J Water Resour Prot. 2018;10:762–79. https://doi.org/10.4236/jwarp.2018.108043.
15. Goldberg N. Air conditioning, heating, and ventilation. In: Avallone EA, Baumeisterm T, editors. Mark's standard handbook for mechanical engineers. 10th ed. New York: McGraw-Hill; 1996. pp. 12–86.
16. Trenberth KE, Caron JM, Stepaniak DP, et al. Evolution of El Niño–Southern Oscillation and global atmospheric surface temperatures. J Phys Res. 2002. https://doi.org/10.1029/2000JD000298.
17. Jaramillo A, Dominguez C, Raga G, Quintanar AI. The combined QBO and ENSO Influence on Tropical Cyclone Activity over the North Atlantic Ocean. Atmosphere. 2021;12(12):1588. https://doi.org/10.3390/atmos12121588.
18. Caballero R. Physics of the Atmosphere. Bristol: IOP Publishing Ltd; Bristol; 2014. pp. 2-1–2-33, 3-1–3-29, 6-1–6-5.
19. Lin KH, Van Ness HC, Abbott MM. Thermodynamics. In: Crawford HB, Eckes BE, editors. Perry's Chemical Engineers Handbook. 6th ed. New York: Mc Graw-Hill; 1984. pp. 4–52.

Publisher's Note